

Reconfigurable Planar Capacitive Coupling in Substrate-Integrated Coaxial-Cavities Filters

Akash Anand, *Student Member, IEEE*, and Xiaoguang Liu, *Member, IEEE*

Abstract—This paper presents design strategies and experimental demonstrations of frequency and bandwidth tunable filters with adjustable transmission zeros (TZ). By the judicious choice of the absolute and relative strength of magnetic and electric coupling coefficients, we demonstrate 1) tunable bandwidth and the ability of maintaining either a constant absolute bandwidth or a constant fractional bandwidth; 2) adjustable transmission zero location at a prescribed bandwidth; 3) the ability to switch off the filter with high isolation. Filter design methodologies based on a new dispersive coupling structure are presented using lumped models, coupling matrix, and full-wave simulations. We also demonstrate with this planar capacitive coupling, it is convenient to realize cross-coupling in higher order filters to produce additional TZs for rejecting spurious resonances or interferences. Fabricated two-pole filters with one or two TZs and four-pole filters with three or four TZs validate the filter design. A two-pole filter with tunable center frequency and tunable bandwidth along with a four-pole filter with tunable center frequency and tunable transmission zeros are also demonstrated.

Index Terms—coaxial cavity resonator, coaxial cavity filter, combine filter, evanescent-mode filter, tunable bandwidth, tunable filters, tunable resonators

I. INTRODUCTION

OVER the past decades, highly selective cavity filters with low insertion loss filtered signals without much sacrifice in system performance [1]. With today's diverse technology applications, interest in other filter technologies and topologies continues, including in the recent growing area of tunable filters. Various works show promising results in some areas of performance but usually at the cost of performance in other parameters. For example, substrate-integrated waveguide (SIW) cavity filters have gained considerable interest for RF/microwave systems for their easy fabrication and low cost compared to traditional air-filled cavities [2], [3]. But this comes at the expense of lower unloaded quality factor (Q_u) due to substrate loss.

In coupled resonator filters, the frequency response is determined by the external and internal coupling strength. For an evanescent-mode cavity filter, Fig. 1(a) shows both magnetic coupling, through openings in the cavity wall (iris), and electric coupling, where a conductive metal probe is suspended between the cavity's center posts. Traditionally in

This paper is an expanded paper from the IEEE Wireless and Microwave Technology Conference (WAMICON) held on June 6, 2014 in Tampa, FL.

A. Anand and X. Liu are with the Department of Electrical and Computer Engineering, University of California at Davis, Davis, CA 95616 USA (e-mail: akaanand@ucdavis.edu; lxgliu@ucdavis.edu).

The authors would like to thank the National Defense Science and Engineering Graduate Program and the University of California, Davis Hellman Fellows Program for supporting this research.

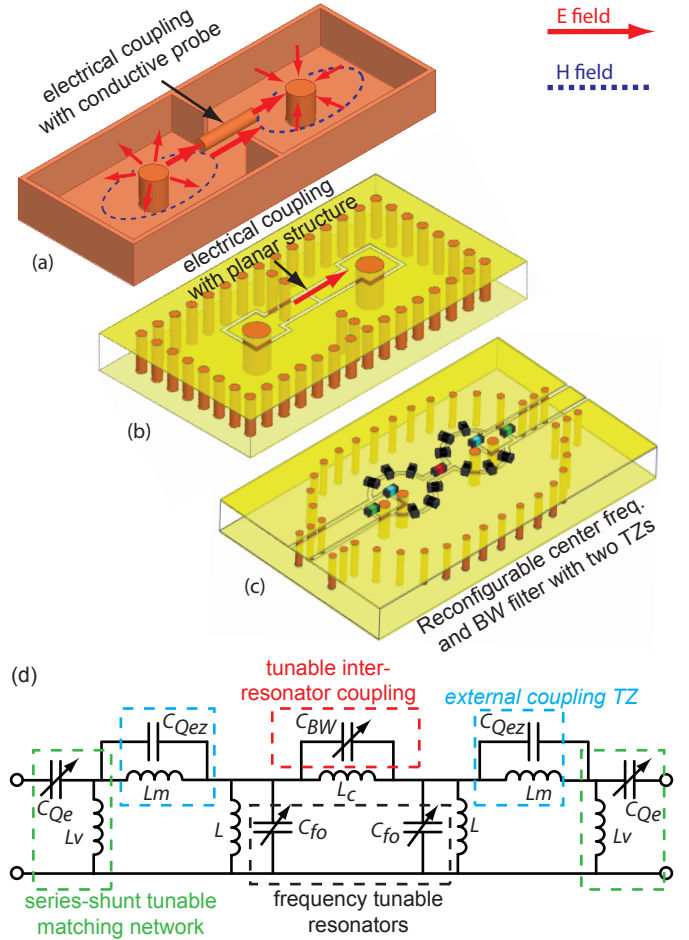


Fig. 1. (a) Coaxial-cavity filter with traditional electrical coupling and (b) proposed substrate integrated filter with planar electrical coupling. (c) Tunable filter with lumped components and (d) equivalent circuit model for tunable filter.

such cavities, coupling between resonators is predominantly magnetic (inductive) since it is easier to implement compared to electrical (capacitive) coupling probes. For this reason, other methods for electrical coupling are presented in [4]–[7]. In evanescent-mode (EVA) resonators, one end of the center conductor is shorted while the other end is capacitively loaded [1]. Magnetic fields are stronger in the shorted end and electric fields stronger in the loaded end [5]. Thus, with appropriate location of iris openings and spacing of the center conductors, works from [4] and [5] realize mixed electric and magnetic coupling without using conductive probes. To make fabrication even simpler, others use planar structures in SIW filters. For example, [6] uses inter-digital slot-line between resonators

and [7] uses embedded short-ended strip line between two PCB layers to realize electrical coupling. Nevertheless, all of these works present fixed coupling structures.

It is desirable to electrically tune the capacitive coupling to realize reconfigurable BW cavity filters. But little work has been done towards this. For example, work from [8] shows an EVA mode topology with surface mount PIN diodes to tune the coupling discretely. The fabrication for this filter requires precise assembly to align the piezo-actuator with the cavity's post and requires multiple layers to integrate the PIN diodes. Work from [9] shows continuously tunable electrical coupling with surface mount varactors in SIW filters, but this structure is mostly appropriate for bandstop filters. On the other hand, surface mount lumped components in planar filters electrically tune the capacitive coupling easily. For example, numerous planar filters with tunable BW have been presented [10]–[18]. However, SIW filters are still preferred over planar structures for their improved performance in insertion loss. But integrating lumped components into SIW cavities is not as convenient as it is in planar microstrip or co-planar waveguide (CPW) structures.

The authors introduced a new substrate-integrated planar capacitive coupling structure for inter-resonator coupling in [19], where a surface mount varactor tunes the coupling. The authors first show a tunable bandwidth two-pole filter in [19] and later [20] shows higher order filters based on this coupling structure. This paper extends upon the work presented in [19]. While a transmission zero due to dispersive inter-resonator coupling [4], [21], [22] is briefly mentioned in [19], this work presents a more detailed filter design method to place the TZ at a specified location for a prescribed fractional bandwidth (FBW) based on lumped models, coupling matrix, and simulation curves. Further, electrical coupling introduces additional transmission zeroes in higher order cross-coupled filters to sharpen skirt selectivity [23], [24]. We illustrate this with the proposed planar structure integrated in four-pole filters. The external coupling adds yet another TZ above the passband and surface mount components are easily integrated into the filter to tune the center frequency, BW, and external coupling. To validate the filter design, we fabricate and measure two-pole filters with one or two TZs, four-pole filters with three or four TZs, and a two-pole frequency and BW tunable filter with tuning range from 0.55 GHz to 1.1 GHz with a BW of 20–91 MHz at 1.1 GHz, 20–95 MHz at 0.84 GHz, and 34–66 MHz at 0.55 GHz. A four-pole filter with tunable center frequency and tunable transmission zeros is also demonstrated.

II. COAXIAL-CAVITY RESONATOR

The filter in Fig. 1(b) is based on the coaxial cavity resonator presented in [25]. A ring gap on the top surface of a coaxial transmission line, with both ends shorted, isolates the center conductor (post) from the rest of the cavity's top surface. The ring gap also capacitively loads the coaxial cavity. This 3D structure is analogous to planar combline filter where microstrip transmission lines are capacitively loaded. With capacitive loading, the coaxial transmission line is seen as an inductive element and hence resonates like a LC tank [26].

Varactors mounted on the ring gap tunes the center frequency (f_o) of the resonator [27]–[30]. Works from [25] and [31] present theoretical analysis on this resonator which is summarized below in Eqns. (1)–(5).

The angular resonant frequency ω_o is approximated as

$$\omega_o = \frac{1}{\sqrt{LC}} \quad (1)$$

where L is the inductance of the coaxial transmission line (ignoring surface inductance) and $C = C_v + C_o$. C_v is equivalent capacitance of all the frequency tuning varactors (C_{fo}) and C_o is the surface gap capacitance. The inductance is given by

$$L = \frac{Z_o}{\omega} \tan \left(\frac{\omega h \sqrt{\epsilon_r}}{c} \right) \quad (2)$$

where Z_o is the characteristic impedance, h is the height of the cavity, ϵ_r is the dielectric constant, and c is the speed of light in air. For circular cavities, Z_o is given in Eqn. (3a) and for square cavities, Z_o is given in Eqn. (3b),

$$Z_o = \frac{60}{\sqrt{\epsilon_r}} \ln(b/a) \quad (3a)$$

$$Z_o = \frac{60}{\sqrt{\epsilon_r}} \ln \left(1.079 \frac{s}{a} \right) \quad (3b)$$

where a is the radius of the inner conductor, b is the radius of the outer conductor of the circular resonator and s the length of one side of the square cavity's wall.

The unloaded quality factor is approximated as

$$\frac{1}{Q_u} = \frac{1}{Q_c} + \frac{1}{Q_v} \quad (4)$$

where Q_v is the quality factor of the C_{fo} varactors and Q_c is quality factor of just the circular resonator (without C_{fo})

$$Q_c = \frac{\omega_o L}{R_s \left(\frac{h}{a} + \frac{h}{b} + 2 \ln(b/a) \right)} \quad (5)$$

in which R_s is the surface resistance.

III. DISPERSIVE INTER-RESONATOR COUPLING

Fig. 1(b) shows the proposed filter with electric coupling, where the conductive probe from the traditional filter in Fig. 1(a) is moved to the surface as a planar structure which resembles a CPW transmission line. There is a gap in the middle of this CPW line which separates the two resonators. The traditional filter in Fig. 1(a) and proposed filter Fig. 1(b) both still have the same inter-resonator magnetic coupling, where magnetic fields around the center posts couple to each other through the iris opening in the resonators' adjacent wall. Thus, the presented filter has a mixed electric and magnetic inter-resonator coupling structure.

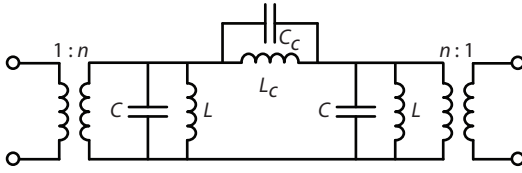


Fig. 2. Lumped model for inter-resonator coupling. The parallel combination of L_c and C_c creates a TZ at $f_{z1} = 1/2\pi\sqrt{L_cC_c}$.

A. Filter Design

In order to design filters with this mixed coupling, we first present a lump model that approximates the inter-resonator coupling and aids in visualizing the TZ that results. Guidelines are then presented to design filters with a specified TZ location at a prescribed FBW based on the lumped model. Since the 3-D filter structure is complex and coupling depends highly on filter dimensions, more accurate design curves are then presented based on full-wave electromagnetic simulator Ansys HFSS.

Since the mixed couplings is dispersive [19], it is possible that the magnetic coupling equals the electric coupling at a certain frequency and a TZ occurs—if two the couplings have opposite signs. Previous works from [4], [6], [7], [21], [22], [32] report this TZ in 3-D structures, which is easier to visualize with the lumped model in Fig. 2. Inductance L and capacitance C model the parallel resonators while L_c and C_c represent the inductive and capacitive coupling [33]. The parallel combination of L_c and C_c creates a TZ (TZ_1) at

$$f_{z1} = \frac{1}{2\pi\sqrt{L_cC_c}}. \quad (6)$$

Consider the case when the electric coupling and magnetic coupling are equal at the center frequency, then TZ_1 occurs at center frequency or $f_{z1} = f_o$. If electric coupling becomes dominant, then TZ_1 moves below the passband: C_c or L_c increases, or the change in electric coupling is greater than change in magnetic coupling if C_c and L_c both change in opposite directions. Conversely, if magnetic coupling becomes dominant, then TZ_1 moves above the passband: C_c or L_c decreases, or the change in magnetic coupling is greater than change in electric coupling if C_c and L_c both change in opposite directions. Table I shows various filters designed with 6% 3-dB FBW but with different TZ_1 locations. For example, for filters with TZ_1 below the passband in Table I, L_c decreases from 47.5 nH to 6.44 nH and TZ_1 moves higher in frequency while C_c increases to keep the same FBW. For filters with TZ_1 above the passband, C_c increases from 0.1 pF to 0.5 pF and TZ_1 moves lower in frequency while L_c decreases to keep the same FBW. Fig. 4 shows S_{21} for selected examples. Based on the above discussion and Table I, we can summarize the following for filters designed at f_o with a fixed FBW:

- (a) When electric coupling is dominant, TZ_1 is below the passband.
- (b) When magnetic coupling is dominant, TZ_1 is above the passband.

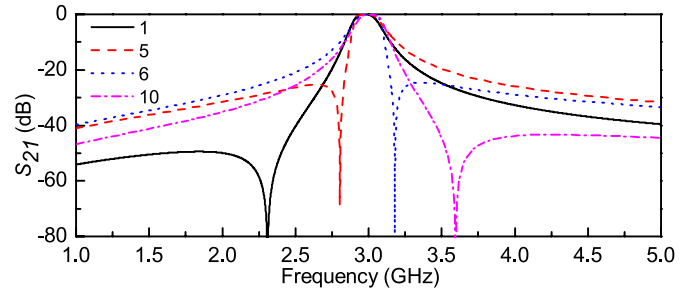


Fig. 3. Selected examples from Table I with filters designed with 6% FBW but different TZ_1 locations based on lumped model from Fig. 2.

- (c) Below the passband, TZ_1 moves to higher frequency (closer to the passband) as magnetic coupling increases (L_c decreases).
- (d) Above the passband, TZ_1 moves to lower frequency (closer to the passband) as electric coupling increases (C_c increases).

TABLE I
FILTERS DESIGNED WITH 6% 3-DB FBW AT $f_o = 3$ GHZ BUT WITH DIFFERENT TZ_1 LOCATIONS BASED ON LUMPED MODEL FROM FIG. 2

filter	n	L (nH)	C (pF)	C_c (pF)	L_c (nH)	TZ_1 (GHz)
TZ_1 below the passband						
1	5	3.2	0.85	0.1	47.5	2.31
2	5	3.2	0.85	0.2	18.2	2.64
3	5	3.2	0.85	0.3	11.4	2.72
4	5	3.2	0.86	0.4	8.23	2.77
5	5	3.2	0.86	0.5	6.44	2.81
TZ_1 above the passband						
6	5	3.2	0.91	0.5	5.01	3.18
7	5	3.2	0.91	0.4	6.16	3.21
8	5	3.2	0.91	0.3	7.97	3.26
9	5	3.2	0.91	0.2	11.4	3.34
10	5	3.2	0.91	0.1	19.6	3.60

The inter-resonator electric and magnetic couplings are defined as k_E and k_M . The total inter-resonator coupling (k) is then the sum of k_E and k_M [33],

$$k = \frac{k_M + k_E}{1 + k_M k_E} \approx k_M + k_E \quad (7)$$

for narrow band filters and k can be extracted from

$$k = \pm \frac{f_1^2 - f_2^2}{f_1^2 + f_2^2} \quad (8)$$

where f_1 and f_2 are the eigen frequencies of the coupled resonators. Since the signs of magnetic (+) and electric (−) coupling are opposite [19], k can be either positive, negative, or zero.

According to [34], the required values for k and external coupling (Q_e) for a particular filter design is

$$k_{i,i+1} = \frac{FBW}{\sqrt{g_i g_{i+1}}} \text{ for } i = 1 \text{ to } (n-1) \quad (9)$$

and

$$Q_{e1} = \frac{g_0 g_1}{FBW} \text{ and } Q_{en} = \frac{g_n g_{n+1}}{FBW} \quad (10)$$

where n is the order of the filter and the g values are given in any standard filter design reference such as [1], [33], [34].

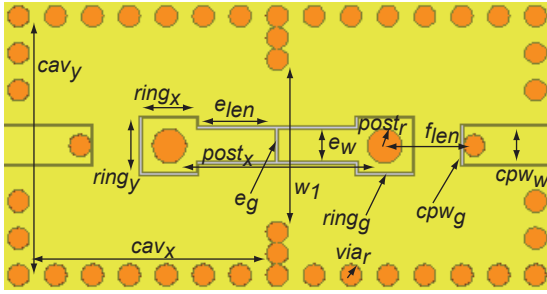


Fig. 4. Two resonators with mixed electric and magnetic inter-resonator coupling and labeled dimensions.

Fig. 4 shows two resonators with inter-resonator coupling designed around 2.7 GHz with dimensions listed in Table II, where h is the substrate height and ϵ_r is the substrate dielectric constant. Fig. 5(a) shows the HFSS simulated k versus e_w (width of the electrical coupling CPW) at various magnetic wall openings w_1 . The electric coupling becomes stronger (more negative) as e_w increases. The magnetic coupling increases as w_1 or the iris opening becomes larger. A CPW transmission line is used as the input/output feeds. The CPW transmission line extends inside the cavity where a via shorts it to the bottom. Current flowing through the CPW shorting via creates magnetic fields that couples with the magnetic fields of the center post. A similar feed structure is analyzed in more details in [35]. Fig. 5(b) shows Q_e versus f_{len} , where f_{len} is the distance between center post and the CPW shorting via shown in Fig. 4. Thus, for a prescribed FBW, k maps to w_1 and e_w in Fig. 5(a) and Q_e maps to f_{len} in Fig. 5(b).

TABLE II
VALUES FOR RESONATORS WITH MIXED INTER-RESONATOR COUPLING
LABELED IN FIG 4.

parameter	value	parameter	value
cav_x	22 mm	cpw_w	3.5 mm
cav_y	22 mm	cpw_g	0.18 mm
h	6.35 mm	f_{len}	10 mm
$ring_x$	5.0 mm	e_{len}	14.51 mm
$ring_y$	5.0 mm	e_g	0.26 mm
$ringg$	0.26 mm	e_w	1.0 mm
$post_r$	1.59 mm	w_1	20.0 mm
$post_x$	20.0 mm	ϵ_r	2.2
via_r	1.01 mm		

A filter with prescribed FBW and flexible TZ_1 location can be designed based on the guidelines from the lumped model. For example, when TZ_1 is above the passband, increasing e_w moves TZ_1 lower in frequency. Conversely, when TZ_1 is below the passband, increasing w_1 moves TZ_1 higher in frequency. For a given e_w or w_1 , the corresponding w_1 and e_w is chosen according to Fig. 5(a) to keep constant $|k|$. Note that k can take negative values at larger e_w . When k is negative, electric coupling is stronger and TZ_1 is below the passband, while when k is positive, magnetic coupling is stronger and TZ_1 is above the passband.

Alternatively, [23] and [36] present coupling matrix theory to model filters and provide design guidelines to generate the coupling matrix at fixed frequencies. But dispersive coupling filters need frequency depended coupling matrix to accurately

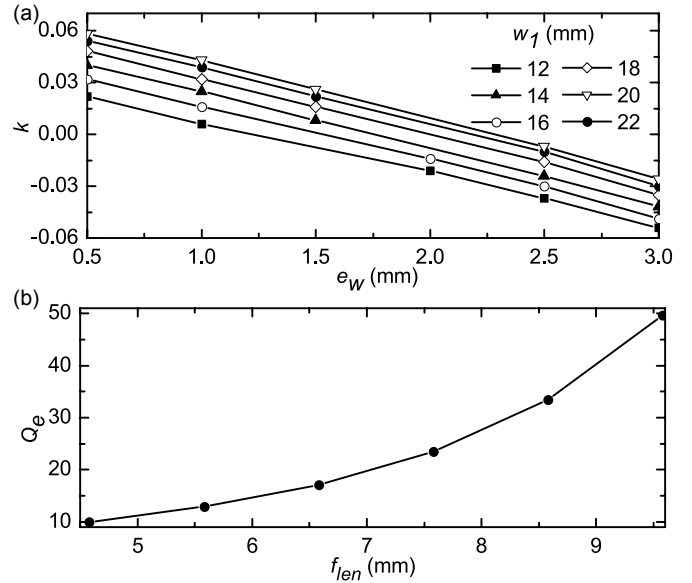


Fig. 5. Simulated (a) k versus e_w at various w_1 values and (b) Q_e versus f_{len} around 2.7 GHz.

model the frequency response. These frequency dependent inter-resonator coupling parameters can be simulated and extracted from HFSS. The steps below give an irritative design procedure to design filters with frequency depended coupling matrix.

- 1) Generate the coupling matrix for a filter with desired specifications without dispersive coupling based on standard coupling matrix design in [23] and [36].
- 2) A series of frequency dependent inter-resonator coupling $k(\omega)$ curves for different FBW can be generated using HFSS. Extract the inter-resonator coupling $m(\omega)$ values from simulated $k(\omega)$ curves.
- 3) Re-optimize coupling matrix values other than the dispersive inter-resonator coupling $m(\omega)$ using numerical simulations (s-parameter), such as MATLAB.
- 4) Repeat steps 2 and 3 to get the desired FBW and TZ location

Examples of such matrix design is presented in Section III-B and section III-C along with simulated and measured results.

B. Two-Pole Filter Example

To illustrate examples of dispersive coupling matrix, two two-pole filters are designed based on guidelines from section III-A: filter M_1 has 6.3% 3-dB FBW and filter M_2 has 8.0% 3-dB FBW around 2.75 GHz. Fig. 6(c) shows the simulated k versus frequency for the two filters, where a second order polynomial $k_{12}(\omega)$ fits the simulation data. A TZ (TZ_1) occurs when $k_{12} = 0$. For M_1 , $k_{12} = 0$ is below the passband around 2.1 GHz and for M_2 , $k_{12} = 0$ is above the passband around 3.6 GHz. Eqns. 11 and 12 shows the coupling matrix with frequency dependent inter-resonator coupling $m_{12}(\omega)$ extracted from $k_{12}(\omega)$. Fig. 6(a) and (b) shows the fabricated filters with SMA connectors. The dimensions are the same as those listed in Table II, except for M_1 , $f_{len} = 8.28$ mm, $e_w = 3$ mm and $w_1 = 14$ mm, and for

M_2 , $f_{len} = 8.08$ mm, $e_w = 1$ mm and $w_1 = 22$ mm. Fig. 6(d) and (e) plots the coupling matrix along with simulated and measured data. Simulated and measured insertion loss in the passband are 0.58 dB and 0.45 dB for M_1 and 0.41 dB and 0.38 dB for M_2 .

$$M_1(\omega) = \begin{bmatrix} 0 & 0.698 & 0 & 0 \\ 0.698 & 0 & m_{12}(\omega) & 0 \\ 0 & m_{12}(\omega) & 0 & 0.698 \\ 0 & 0 & 0.698 & 0 \end{bmatrix} \quad (11)$$

$$\begin{aligned} m_{12}(\omega) &= k_{12}(\omega) \times FBW \\ &= -0.007 \left(\frac{\omega}{10^9} \right)^2 + 0.070 \frac{\omega}{10^9} + 0.354 \end{aligned}$$

$$M_2(\omega) = \begin{bmatrix} 0 & 0.774 & 0 & 0 \\ 0.774 & 0 & m_{12}(\omega) & 0 \\ 0 & m_{12}(\omega) & 0 & 0.774 \\ 0 & 0 & 0.774 & 0 \end{bmatrix} \quad (12)$$

$$\begin{aligned} m_{12}(\omega) &= k_{12}(\omega) \times FBW \\ &= -0.005 \left(\frac{\omega}{10^9} \right)^2 + 0.1150 \frac{\omega}{10^9} + 0.0325 \end{aligned}$$

C. Higher Order Filters with Cross-Coupling

In addition to designing filters with mixed coupling in adjacent resonators, we can use the presented structure in cross-coupled resonators to design higher order filters with additional TZs. For example, Fig. 7 shows the coupling schematic for four-pole cross-coupled filters. Filters in Fig. 7(a) and (b) have all inductive coupling between resonators except for the capacitive coupling between resonators 1 and 4 in Fig. 7(a) and between resonators 2 and 3 in Fig. 7(b). In both filters, the main line path (1, 2, 3, and 4) and cross coupling path (1 and 4) are out of phase and add destructively to create a pair of TZs [37]. This is verified with coupling matrix given in Eqn. 13 and plotted in Fig. 8. Both filters have the same coupling matrix except for the coupling sign between resonators 1 and 4 and between resonators 2 and 3, which is (+) when the coupling is inductive and (-) when the coupling is capacitive.

$$M_3 = \begin{bmatrix} 0 & 1.02 & 0 & 0 & 0 & 0 \\ 1.02 & 0 & 0.856 & 0 & \mp 0.220 & 0 \\ 0 & 0.856 & 0 & \pm 0.786 & 0 & 0 \\ 0 & 0 & \mp 0.786 & 0 & 0.856 & 0 \\ 0 & \mp 0.220 & 0 & 0.856 & 0 & 1.02 \\ 0 & 0 & 0 & 0 & 1.02 & 0 \end{bmatrix} \quad (13)$$

A third TZ is generated if mixed cross-coupling between resonators 1 and 4, instead of purely inductive or capacitive, is used [5], [38]. Fig. 7(c) and (d) show the schematic for mixed cross-coupling between resonator 1 and 4. This work qualitatively discusses the presence of all three TZs while additional analysis is presented in [5]. In the passband, the magnitude of main line path with resonators 1, 2, 3, and 4 (four-pole filter) is dominant compared to magnitude of the cross-coupled resonators 1 and 4 (two-pole filter). As ω moves away from the passband, the magnitude of the four-pole filter

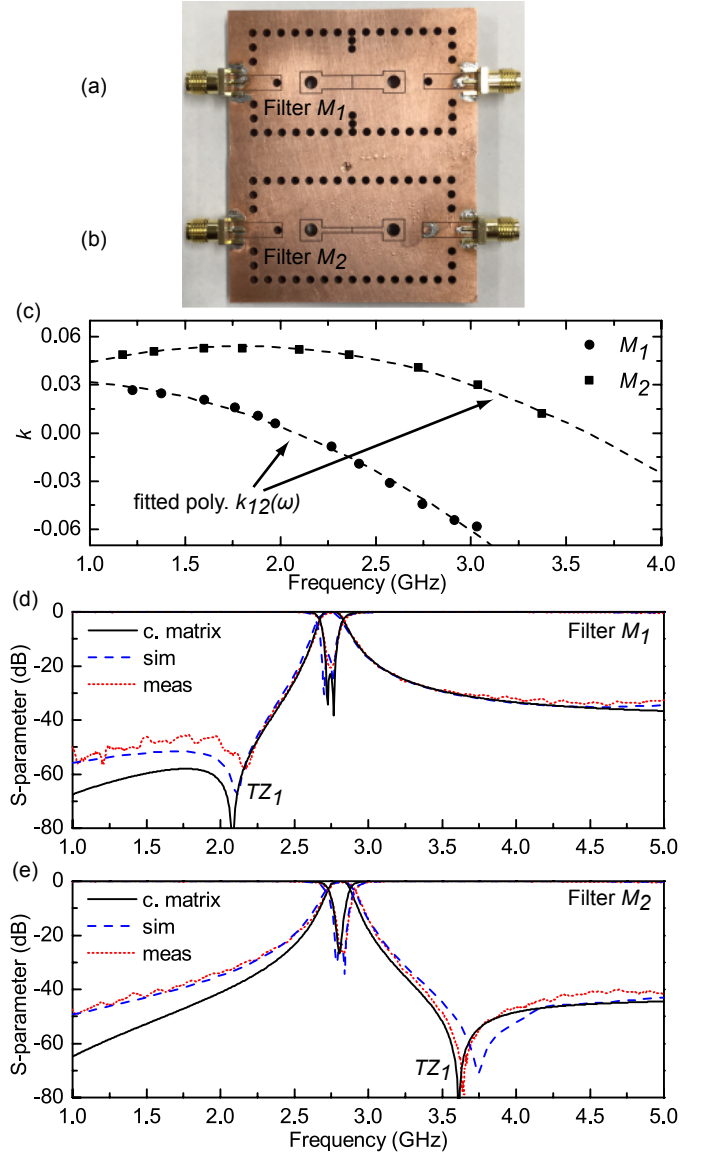


Fig. 6. Fabricated two-pole filters (a) M_1 and (b) M_2 and (c) HFSS simulated dispersive inter-resonator k for designed filters. Plots of measured, simulated and coupling matrix in (d) Eqn. 11 and (e) Eqn. 12.

(main line path) falls faster than the magnitude of the two-pole filter (cross-coupling path). A pair of real frequency TZ (TZ_2 and TZ_3) results when the magnitude of the main line coupling and the magnitude of the cross-coupling are the same at frequencies f_{z2} and f_{z3} . Beyond f_{z2} and f_{z3} , the two-pole filter (cross-coupling path) is dominant and TZ_1 appears at f_{z1} due to the inter-resonator coupling (same TZ from section III-A). TZ_1 can be placed anywhere below TZ_2 or above TZ_3 in Fig. 8.

The design procedure for the mixed cross-coupling is the same as that in section III-A, where the magnitude of cross-coupling from the coupling matrix maps to extracted coupling curves from simulation. Eqns. 14 and 15 gives the coupling matrix for two designed filters, M_4 and M_5 , where frequency dependent $m_{14}(\omega)$ is extracted from HFSS simulation, similar to $m_{12}(\omega)$ in Eqns. 11 and 12. When mixed cross-coupling is

$$M_4(\omega) = \begin{bmatrix} 0 & 1.164 & 0 & 0 & 0 & 0 \\ 1.164 & 0 & 0.957 & 0 & m_{14}(\omega) & 0 \\ 0 & 0.957 & 0 & 0.851 & 0 & 0 \\ 0 & 0 & 0.851 & 0 & 0.957 & 0 \\ 0 & m_{14}(\omega) & 0 & 0.957 & 0 & 1.164 \\ 0 & 0 & 0 & 0 & 1.164 & 0 \end{bmatrix} \quad m_{14}(\omega) = -0.054 \frac{\omega}{10^9} + 0.623 \quad (14)$$

$$M_5(\omega) = \begin{bmatrix} 0 & 1.114 & 0 & 0 & 0 & 0 \\ 1.114 & 0 & 0.957 & 0 & m_{14}(\omega) & 0 \\ 0 & 0.957 & 0 & -0.843 & 0 & 0 \\ 0 & 0 & -0.843 & 0 & 0.957 & 0 \\ 0 & m_{14}(\omega) & 0 & 0.957 & 0 & 1.114 \\ 0 & 0 & 0 & 0 & 1.114 & 0 \end{bmatrix} \quad m_{14}(\omega) = -0.060 \frac{\omega}{10^9} + 1.1843 \quad (15)$$

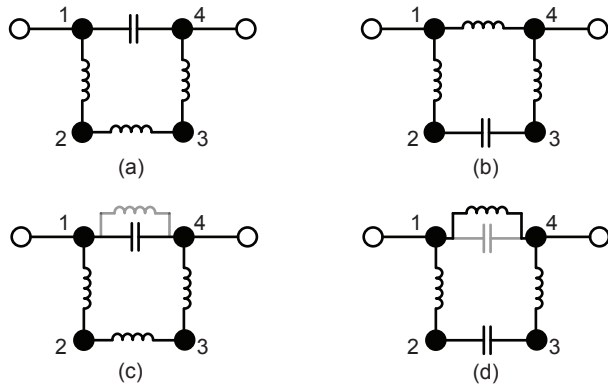


Fig. 7. Coupling schematic for four-pole cross-coupled filters with (a) capacitive cross coupling, (b) inductive cross-coupling, (c) stronger capacitive with weaker inductive cross-coupling and (d) stronger inductive with weaker capacitive cross-coupling.

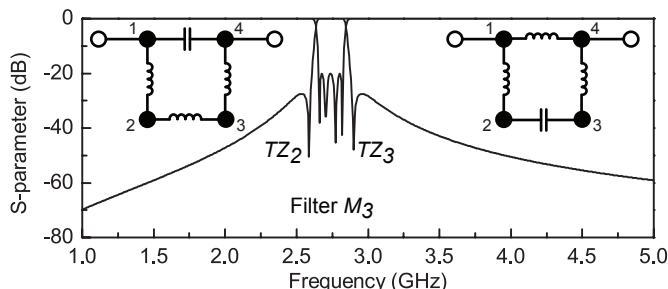


Fig. 8. Both capacitive and inductive cross-coupling from Fig. 7(a) and (b) have two TZs, one on each side of the passband.

strongly electric, TZ_1 will be below the passband and when the mixed cross-coupling is strongly magnetic, TZ_1 will be above the passband (analogues to Fig. 6(d) and (e)). Fig. 10(a) and Fig. 10(b) plots the coupling matirx along with simulated and measured data. The figure also labels the location of TZ_1 , TZ_2 , and TZ_3 . Fig. 9(a) and Fig. 9(b) show the fabricated filter along with the filter dimensions and SMA connectors. All other dimensions of the filter are same as the dimensions labeled in Fig. 4 and listed in Table II. Simulation shows M_4 has 8.6% FBW and 0.45 dB insertion loss at 2.7 GHz while measurement shows 9.3% FBW and 0.43 dB insertion loss. Simulation shows M_5 has 8.1% FBW and 0.46 dB insertion

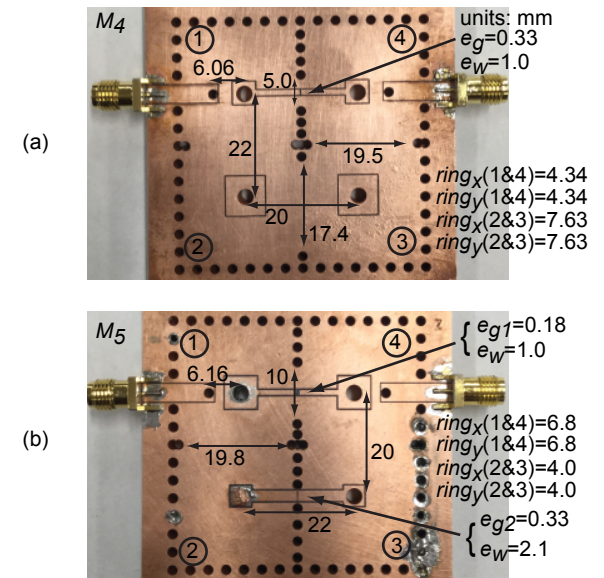


Fig. 9. Fabricated four-pole filter (a) M_4 and (b) M_5 with mixed electric and magnetic coupling.

loss at 2.6 GHz while measurement shows 7.6% FBW and 0.90 dB insertion loss. Incomplete plating of some of the vias degraded insertion loss in M_5 compared to simulation.

IV. EXTERNAL COUPLING TZ

Fig. 11(a) shows a modified lumped model from section III-A, where mutual inductance between L'_v models the external coupling. Another capacitor, C_{Qez} is added in parallel with the mutual inductance. If the mutual inductance is modeled with an equivalent π -network [33], then Fig. 11(a) can be represented as Fig. 11(b), where L includes one of the L'_v and one of the shunt L_m inductors and L_v includes the other shunt L_m inductor. The series parallel combination of L_m and C_{Qez} creates another pair of TZ, (TZ_4), located at

$$f_{z4} = \frac{1}{2\pi\sqrt{L_m C_{Qez}}}. \quad (16)$$

Fig. 12(a) shows the first method to realize C_{Qez} , where part of the CPW feed line extends further into the cavity

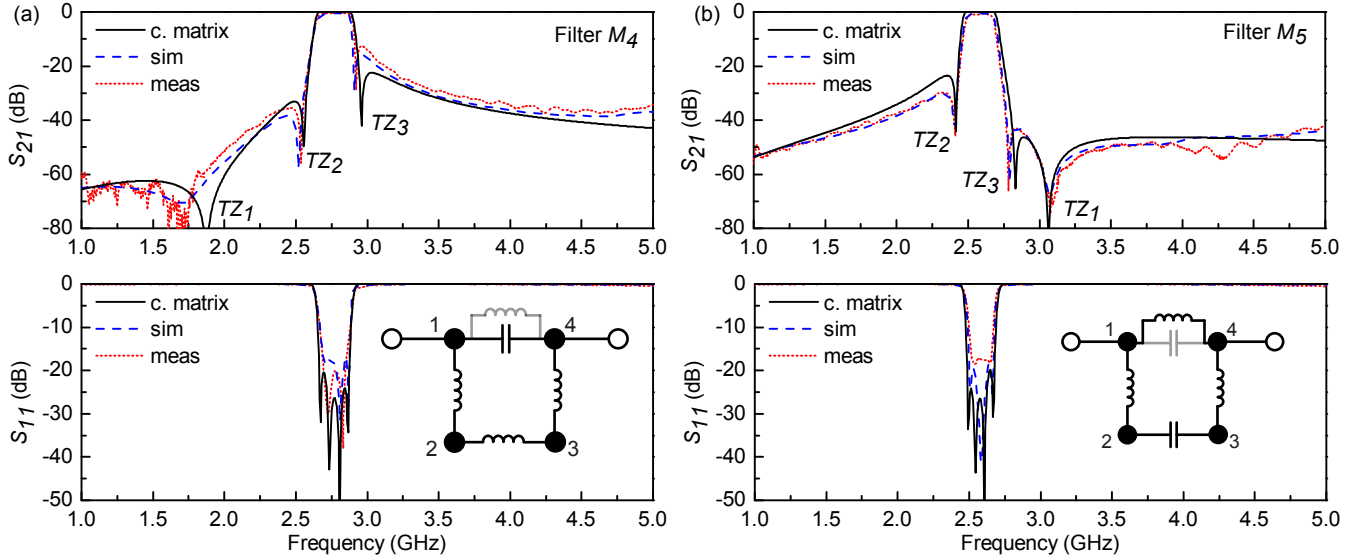


Fig. 10. Plots of measured, simulated, and coupling matrix in (a) Eqn. 14 and (b) Eqn. 15. Compared to Fig. 8, a third notch (TZ_1) is created (a) below the passband for stronger electric coupling (M_4) and (b) above the passband for stronger magnetic coupling (M_5).

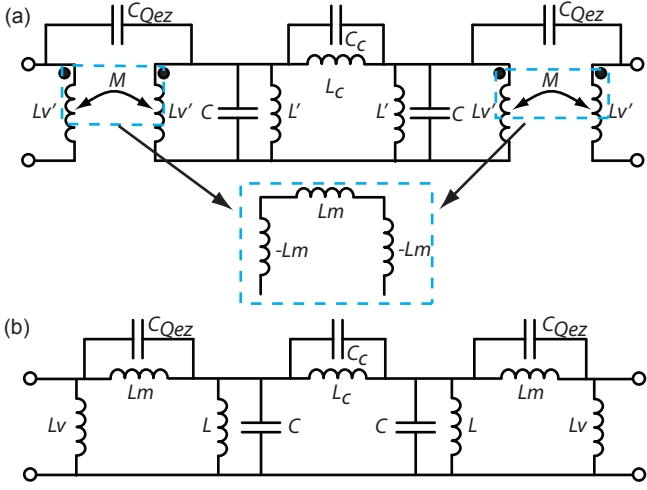


Fig. 11. (a) Lumped model for two-pole filter where mutual inductance models the external coupling. The mutual inductance are modeled with π -networks and (b) shunt L_m inductance are absorbed into L and L_v . The parallel combination of L_m and C_{Qez} creates TZs at $\omega_m = 1/\sqrt{L_m C_{Qez}}$

and overlaps with the square ring gap. Some of the input/output energy flows directly into the resonator through this overlap capacitance (C_{Qez}) while some energy couples in parallel through the mutual inductance between the center post and CPW shorting post. Measured and simulated results in Fig. 12(b) shows a two-pole filter with TZ_4 above the passband and TZ_1 below the passband. Simulation shows 5.5% FBW and 0.86 dB insertion loss at 2.8 GHz while measurement shows 5.0% FBW and 0.64 dB insertion loss. The filter is fabricated on a 6.35 mm Rogers TMM3 substrate with dielectric loss tangent of 0.002.

The second method to realize C_{Qez} is to use a lumped capacitor. First the filter is designed according to section III and then C_{Qez} is included and the filter is re-optimized. For example, the four-pole filter M_4 from Fig. 9(a) and

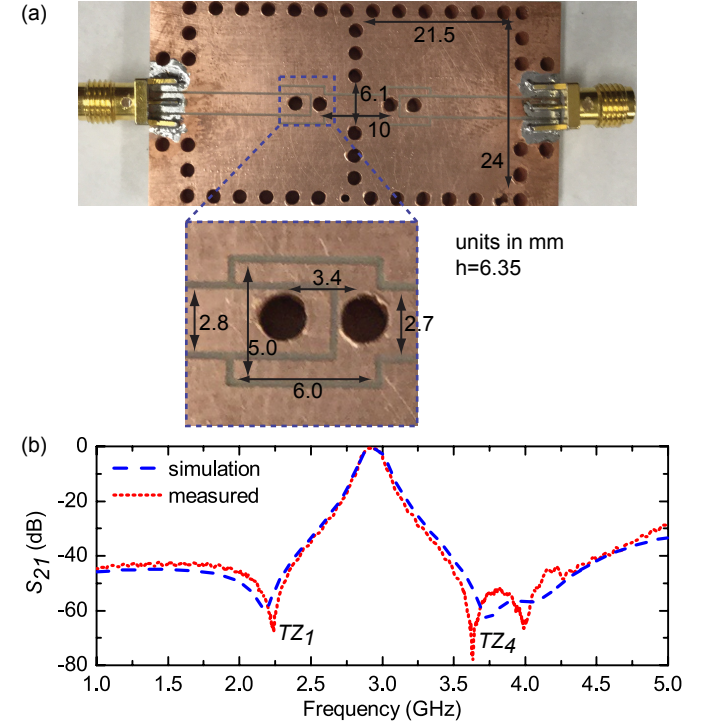


Fig. 12. (a) Fabricated two-pole filter with two zeros where CPW feed line extends further into the cavity and overlaps with the square ring gap, creating some overlap capacitance C_{Qez} and (b) measured and simulated s-parameter.

Eqn. 14 is redesigned to include TZ_4 . Fig. 13(a) shows the fabricated filter with a close-up view of the surface mount C_{Qez} capacitor: the CPW feed line extends towards the cavity but doesn't overlap with the ring gap and a lumped capacitor instead couples energy parallel to the mutual inductance. Compared to the first method with overlapping capacitance, this method requires less re-optimization to the initial design before C_{Qez} is added. Mainly, the external coupling parameter

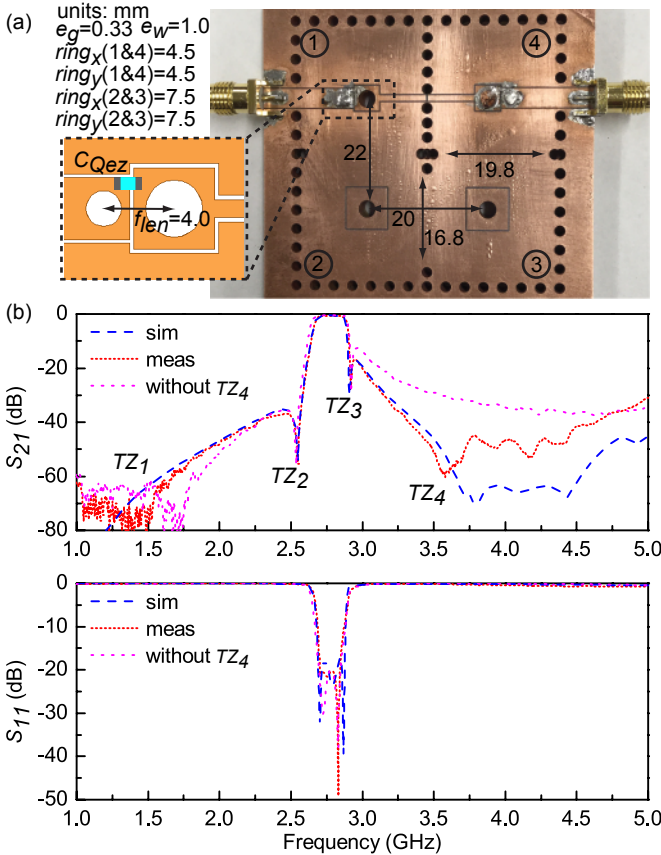


Fig. 13. (a) Fabricated four-pole filter from Fig. 10(a) redesigned to include C_{Qez} and TZ_4 . (b) Measurement and simulation shows improvement in upper stop band rejection with TZ_4 .

f_{len} needs to be redesigned after adding C_{Qez} . Fig. 13(a) shows the modified dimensions. The upper passband rejection improves when TZ_4 is included in Fig. 13(b) compared to same filter without TZ_4 . Simulation shows 7.8% FBW and 0.59 dB insertion loss at 2.7 GHz while measurement shows 8.2% FBW and 0.64 dB insertion loss.

V. RECONFIGURABLE FILTER

A. Tunable BW Filter Design

Fig. 1 and Fig. 14 show that the proposed filter is easily integrated with lumped elements to realize a reconfigurable filter. Fig. 1(d) shows the equivalent lumped model for the reconfigurable filter. Varactors C_{fo} tunes the center frequency, varactor C_{BW} tunes the BW, varactor C_{Qe} tunes the external coupling, and capacitors C_{Qez} produces TZ_4 .

Work from [19] shows Q_u up to 200 for frequency-tunable filters while using only C_{fo} varactors. Adding C_{BW} in the inter-resonator coupling path degrades Q_u even more. So, to minimize this loss and still achieve BW tuning, k_M is designed to be the dominant inter-resonator coupling path so that most of the electromagnetic energy flows through the magnetic fields instead of the lossy varactors. From the design guidelines in section III-A, a strongly magnetic coupled filter is designed. Fig. 15(a) shows k versus center frequency for various C_{BW} . Fig. 15(b) shows the range of FBW solved

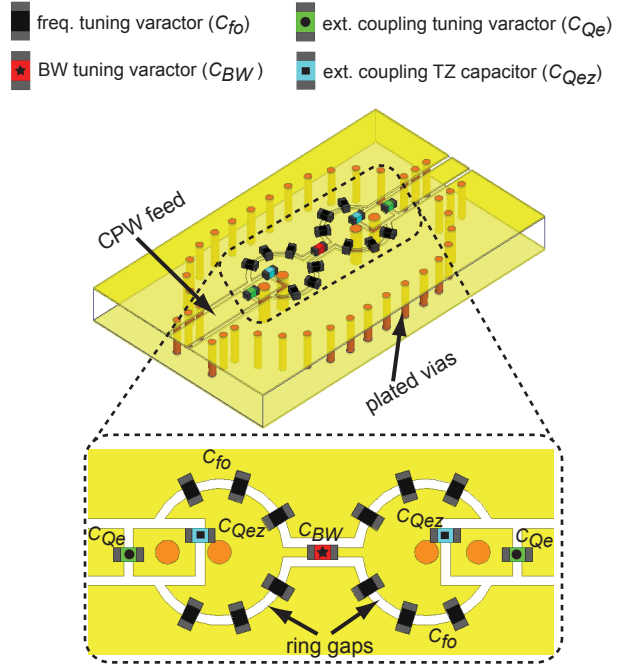


Fig. 14. Tunable two-pole filter and close up of top surface showing the various integrated lumped components and (b) equivalent lumped model.

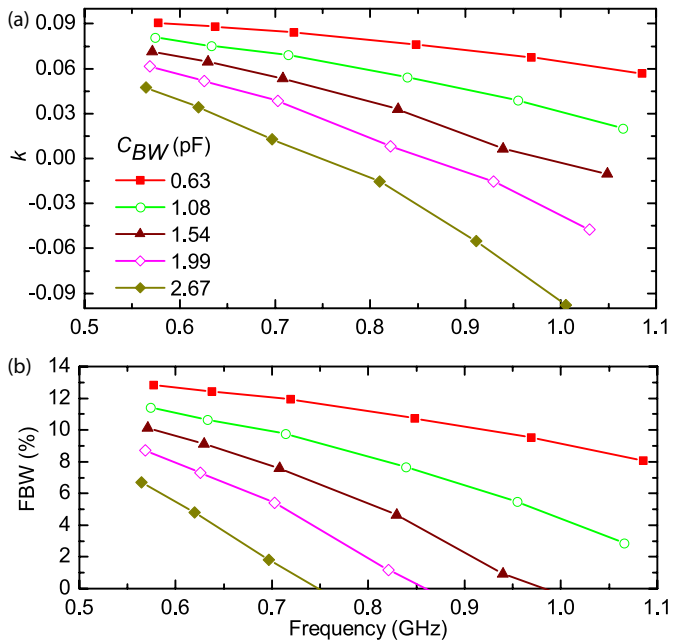


Fig. 15. HFSS simulation for (a) k versus frequency and (b) FBW solved from Eqn. 9 for a two-pole butterworth filter.

from Eqn. 9 for a butterworth filter design. Since it is desired that k_M is dominant, only the FBW corresponding to the positive values on k are plotted. Theoretically, this two-pole filter can achieve a FBW of 0–8% around 1.1 GHz and 7–13% FBW around 0.55 GHz, if not limited by Q_e . The range of FBW at all frequencies is bounded by $C_{BW} = 0.63$ pF and $C_{BW} = 2.67$ pF curves.

Fig. 14 shows varactors (C_{Qe}) mounted over slits created in

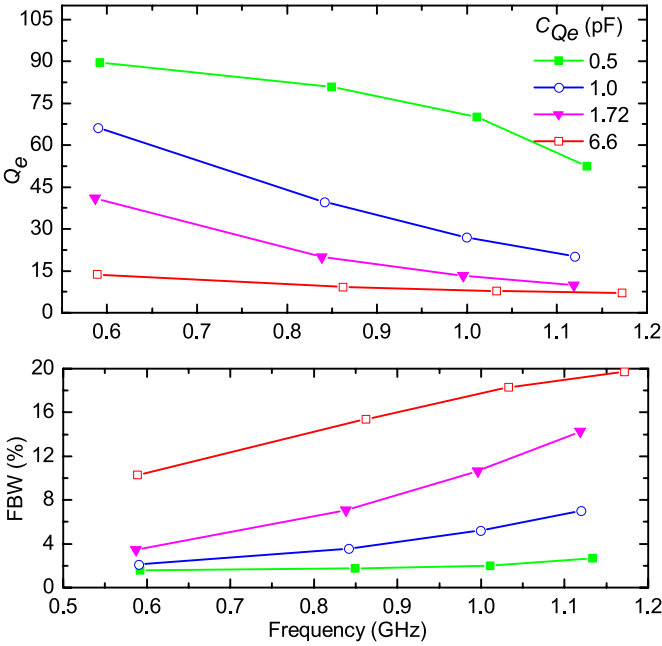


Fig. 16. HFSS simulation for (a) Q_e versus frequency and (b) FBW solved from Eqn. 10 for a two-pole butterworth filter.

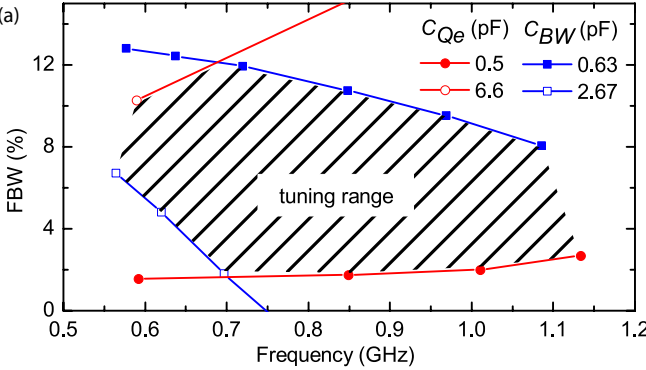


Fig. 17. The shaded region shows the FBW tuning range for the filter as the center frequency tunes from 0.55 GHz to 1.1 GHz.

the CPW line. The lumped model in Fig. 1(d) shows that C_{Qe} and L_v act as a series-shunt matching network. Thus, tuning C_{Qe} varies the input impedance and tunes Q_e . Fig. 16(a) shows HFSS simulation of Q_e versus frequency as C_{Qe} is tuned from 0.5 pF to 6.6 pF. The value of Q_e ranges from 15 to 20 around 0.55 GHz and 7 to 52 around 1.1 GHz. Since Q_e is known, FBW is extracted from Eqn. (10) and plotted in Fig. 16(b). This gives the range of FBW of the filter, if not limited by k .

The tuning range for FBW presented in Fig. 15 and Fig. 16 were based on k and Q_e independently. The actual tuning range of the filter is given when the effects of both k and Q_e is considered together. Thus the extreme values of $C_{BW} = 0.63$ pF and $C_{BW} = 2.67$ pF along with the extreme values of $C_{Qe} = 0.5$ pF and $C_{Qe} = 6.6$ pF are plotted together in Fig. 17. The tuning range of the filter is bounded (shaded region) by the four curves.

HFSS simulation in Fig. 18 shows BW tuning of the filter

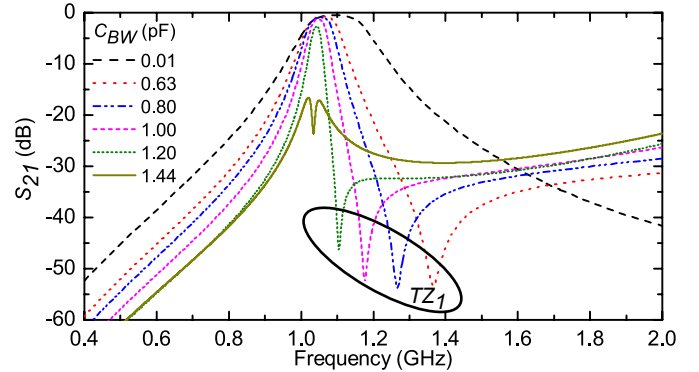


Fig. 18. Simulated tunable BW filter from Fig. 14 without C_{Qez} . Increasing C_{BW} decreases BW and tunes TZ1 closer to the passband.

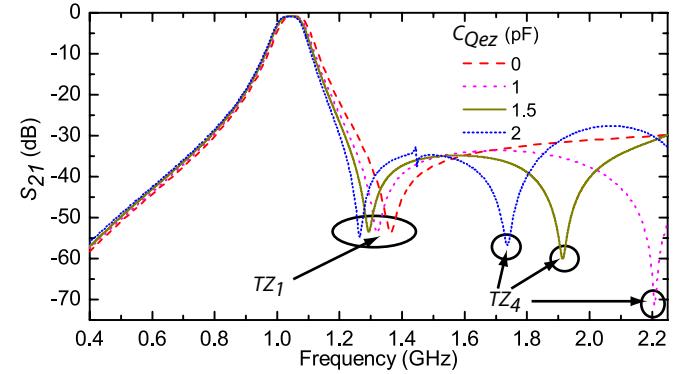


Fig. 19. Tunable filter from Fig. 18 with $C_{BW} = 0.63$ pF shows TZ4 changes significantly with C_{Qez} . Small change in BW and TZ1 is also observed.

around 1.1 GHz without including C_{Qez} capacitor. Initially at $C_{BW} = 0.01$ pF, BW is 170 MHz, and TZ1 is not observed up to 2 GHz. At $C_{BW} = 0.63$ pF, BW is 95 MHz and TZ1 appears at 1.38 GHz. BW decreases further as C_{BW} increases and TZ1 moves closer to the passband. At $C_{BW} = 1.44$ pF, $k_E \approx k_M$ at the center frequency and TZ1 is at f_o : a zero BW filter or the off state of the filter. Fig. 19 shows the simulation result when C_{Qez} is added to realize TZ4. In this case, C_{BW} is kept at 0.63 pF. Increasing C_{Qez} moves TZ4 closer to the passband. Increasing C_{Qez} also decreases the BW and location of TZ1 slightly. The dimensions of the simulated filter is given in section V-B.

B. Tunable BW Filter Validation

The reconfigurable filter from section V-A is fabricated on a Rogers TMM3 board with 5 mm thickness and 0.002 loss tangent. The filter is modified to a double ring structure with additional gaps created on the top surface to mount all the varactors back-to-back. The back-to-back placement of varactors conveniently isolates a dc bias point and improves linearity [39]. Following the guidelines given in [2], vias are drilled in the substrate and plated with copper to form the cavities. The center posts and CPW shorting posts are also created with copper plated vias. The modified filter design is shown in Fig. 20(a) and the fabricated filter with SMA

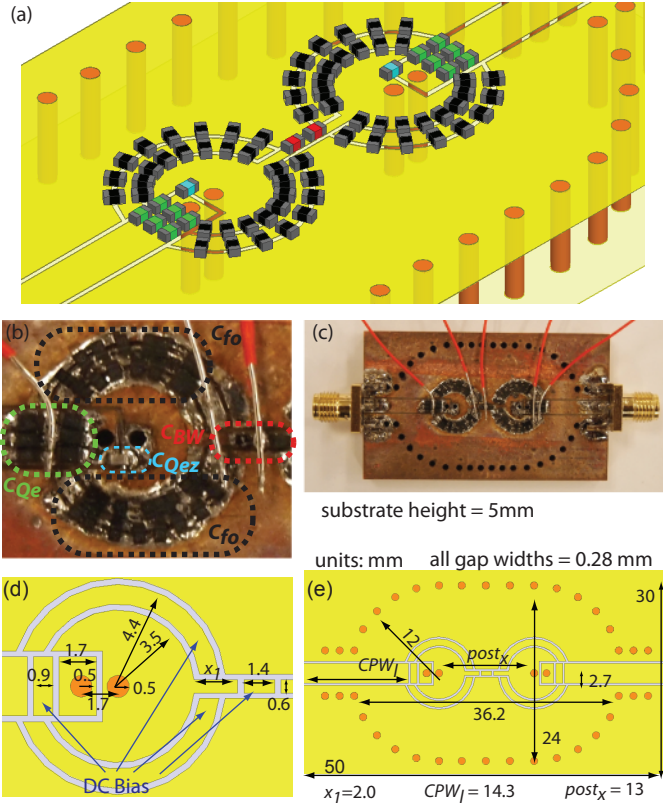


Fig. 20. (a) Designed filter with two ring gaps and back-to-back varactors. Fabricated filter with (b) close-up view and (c) full view. The dimensions of the filter are labeled in (d) and (e).

TABLE III
SURFACE MOUNT LUMPED COMPONENTS

Type	#	Model	Value (pF)	Q @ 50 MHz
C_{fo}	64	Skyworks SMV1405	0.63-2.67	3200
C_{BW}	2	Skyworks SMV1405	0.63-2.67	3200
C_{Qe}	12	Infineon BB857H7902	0.55-6.6	1000
C_{Qez}	2	Johanson Techno. S-Series	1.5	5000

connectors is shown in Figs. 20(b) and (c). Figs. 20(d) and (e) show the dimensions of the board and traces on the top surface. Table. III lists the details of the lumped components used. Additionally, $1\text{-M}\Omega$ resistors are used in the dc bias line to reduce RF loss.

The fabricated filter is first measured without C_{Qez} capacitor. In Fig. 21(a), TZ_1 is initially at 1.5 GHz but moves closer to the passband as C_{BW} increases. The BW decreases from 100 MHz to 20 MHz as C_{BW} increases. Both of these observations are consistent with previous simulation in section V-A. When C_{Qez} is not included, TZ_4 is not seen within 2 GHz frequency range. However, when $C_{Qez} = 1.5 \text{ pF}$ is included, TZ_4 appears around 1.9 GHz in Fig. 21(b), which agrees well with Fig. 19. The location of TZ_4 appears independent of the BW tuning, which makes this TZ ideal for rejecting fixed resonances or interferences.

Fig. 21(c) shows measured S_{21} when the filter is in the off-state: $k_E \approx k_M$ and the two resonators are asynchronously tuned to 0.58 GHz and 1.15 GHz to improve isolation. More

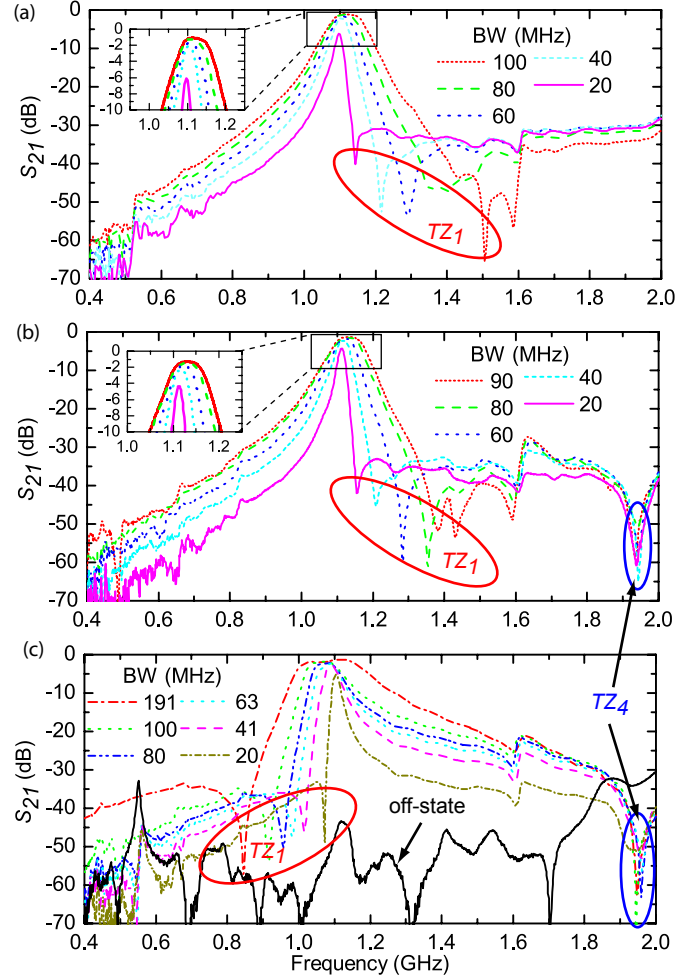


Fig. 21. (a) Measured S_{21} shows both BW and TZ_1 decrease as C_{BW} increases. (b) TZ_4 appears around 1.95 GHz when $C_{Qez} = 1.5 \text{ pF}$ is added. (c) As C_{BW} increases further, TZ_1 moves below the passband while BW increases. An off-state is also measured with the resonators asynchronously tuned.

than 30 dB of off-state isolation is achieved up to 2 GHz. As C_{BW} increases from the off-state, k_E becomes dominant and the BW increases again. TZ_1 has moved below the passband and moves further from the passband as C_{BW} increases. Though a larger BW range is possible for this filter when k_E is dominant, the loss is also higher since more energy is flowing through the C_{BW} varactor.

Fig. 22 shows measured S_{21} and S_{11} for center frequency and BW tuning range. Typical examples of Butterworth and Chebyshev filter responses are shown. This figure can be compared to Fig. 17 where the tuning ranges are predicted from HFSS simulation. Both simulation and measured data shows a center frequency tuning range of about 0.55–1.1 GHz. Table IV compares the simulation versus measured range of BW. The measured and simulated BW ranges match closely. The measured FBW is 6.18–12% at 0.55 GHz, 2.38–11.3% at 0.84 GHz, and 1.77–8.05% at 1.1 GHz. For the measurement, a 10 dB minimum return loss and 20 MHz minimum BW criteria limits the range. Peak insertion loss of 1.28 dB at 1.13 GHz is measured and about 30 dB of out-of-band

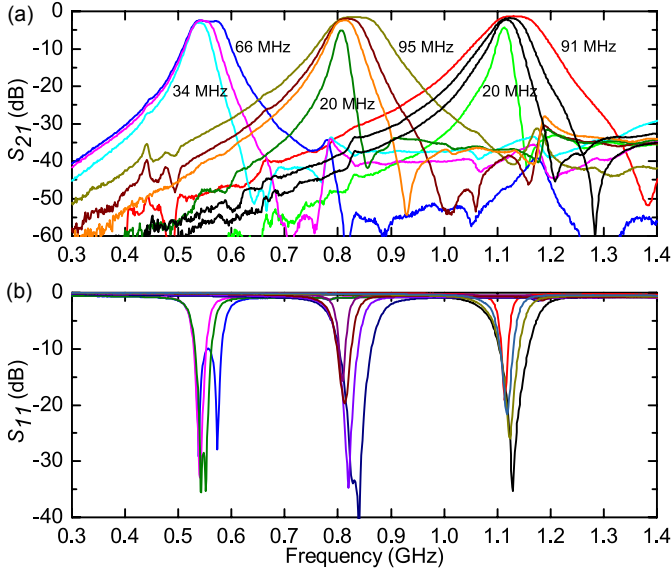


Fig. 22. Measured (a) S_{21} and (b) S_{11} showing both tunable center frequency and tunable BW.

rejection is maintained up to 2 GHz. The extracted Q_u for the resonators is approximately 80 at 0.5 GHz and 200 at 1.1 GHz.

TABLE IV
SIMULATION VERSUS MEASURED BW RANGE

Freq. (Ghz)	Simulation BW (MHz)	Measured BW (MHz)
1.1	30–87	20–91
0.84	14–91	20–95
0.55	37–60	34–66

For some tunable filter applications, maintaining a constant BW or constant FBW maybe desirable. This filter can achieve a constant BW anywhere from 34 MHz to 66 MHz, though a larger BW range is possible with a reduced tuning range such as 20 MHz to 90 MHz BW from 0.7 to 1.13 GHz. As examples, Fig. 23(a) shows 60 MHz 3-dB constant BW tuning with insertions loss between 1.9 dB and 2.3 dB and return loss better than 14 dB, while Fig. 23(b) shows 8% 3-dB FBW tuning with insertion loss between 1.28 dB and 1.7 dB and return loss better than 30 dB. More than 30 dB of out band rejection is maintained in both cases.

C. Tunable TZ Four-Pole Filter

Fig. 24 shows filter M_4 (Fig. 9(a) and Eqn. 14) from section III-C modified to a tunable filter. Two MACOM MA46H120 diodes (Q of 3000 at 50 MHz) are soldered back to back on each resonator to tune the center frequency. The MACOM diodes have a capacitance range of 0.13–1.1 pF. Measured results in Fig. 25 shows the center frequency of four-pole filter tuning from 2.24 GHz to 2.64 GHz.

Similar to the results in section III-C, three TZs are created. However in this case another MACOM MA46H120 diode (C_{TZ}) is used to tune the capacitive cross-coupling between resonator 1 and 4. Since the cross-coupling in filter M_4 is strongly capacitive (section III-C), as C_{TZ} increases the

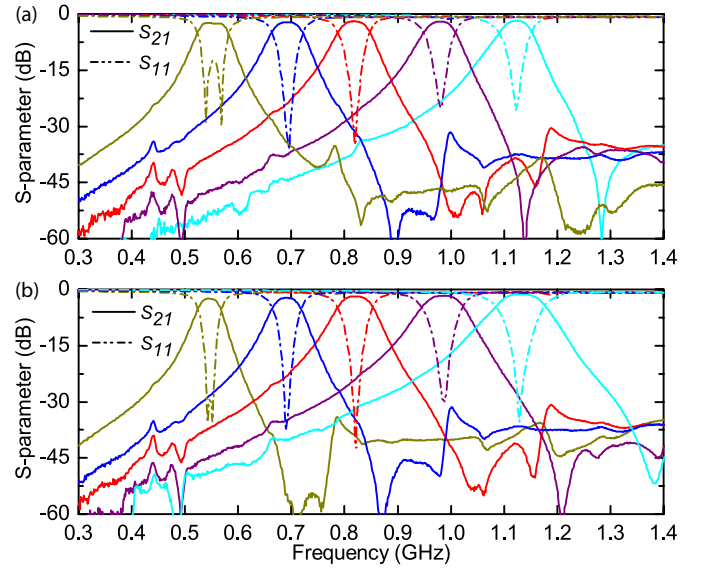


Fig. 23. Measured S_{21} and S_{11} for a (a) 60 MHz constant absolute 3-dB BW and (b) 8% constant 3-dB FBW.

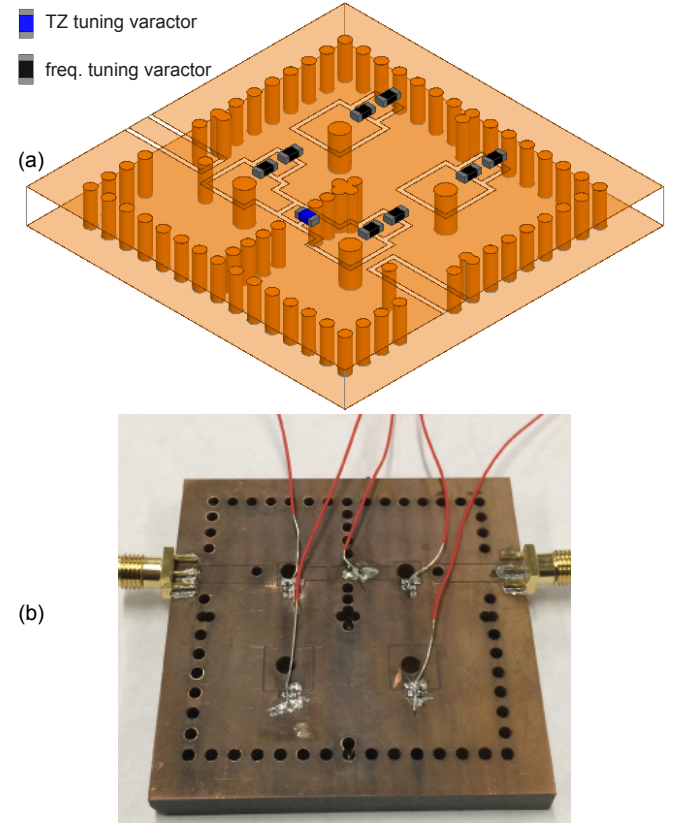


Fig. 24. (a) Designed and (b) fabricated four-pole filter with tunable center frequency and tunable TZs.

magnitude of cross-coupling also increases and TZ_2 and TZ_3 move closer to the passband. Fig. 26 shows the simulated and measured results of the filter while the capacitive cross-coupling is tuned.

Since electric coupling is dominant, TZ_1 is below the

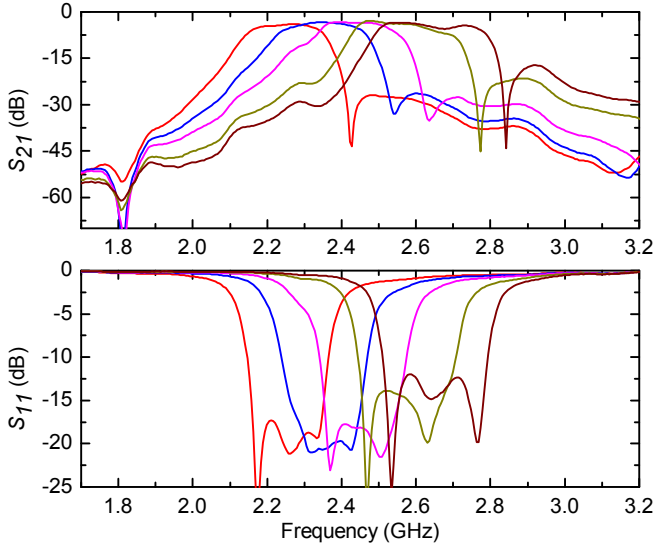


Fig. 25. Measured (a) S_{21} and (b) S_{11} of four-pole filter showing tunable center frequency.

passband, and as the C_{TZ} increases, TZ_1 frequency also increases. This is consistent with Table I where C_c increased to increase TZ_1 frequency.

VI. CONCLUSION

A planar structure for realizing dispersive coupling in substrate-integrated coaxial-cavity filters is presented in this paper. The tunable nature of the coupling structure allows for flexible control of the filter bandwidth and locations of the transmission zeros. Coupling matrix models and design guidelines have been presented to aid the design of such filters, particularly when TZs are needed at desired locations for a prescribed BW. Dispersive Cross-coupling in higher order filter produce additional TZs above and below the passband, in addition to extra TZ produced by the external coupling structure. Fabricated two-pole filters with one or two TZs and four-pole filters with three or four TZs validate the filter design. Conveniently, surface mount components are easily integrated into the planar capacitive structure for bandwidth tuning. A frequency and BW tunable filter shows tuning range from 0.55 GHz to 1.1 GHz with a BW of 20–91 MHz at 1.1 GHz, 20–95 MHz at 0.84 GHz, and 34–66 MHz at 0.55 GHz. A four-pole filter with tunable center frequency and tunable transmission zeros is also demonstrated.

REFERENCES

- [1] C. K. Richard Cameron and R. Mansour, *Microwave Filters for Communication Systems: Fundamentals, Design and Applications*. Hoboken, New Jersey: John Wiley and Sons, 2007.
- [2] K. Wu, D. Deslandes, and Y. Cassivi, "The substrate integrated circuits - a new concept for high-frequency electronics and optoelectronics," in *International Conference on Telecommunications in Modern Satellite, Cable and Broadcasting Service*, vol. 1, Oct 2003, pp. P–III–P–X vol.1.
- [3] K. Entesari, A. Saghati, V. Sekar, and M. Armendariz, "Tunable siw structures: Antennas, vcos, and filters," *IEEE Microwave Magazine*, vol. 16, no. 5, pp. 34–54, June 2015.
- [4] S. Amari and J. Bornemann, "Using frequency-dependent coupling to generate finite attenuation poles in direct-coupled resonator bandpass filters," *IEEE Microwave and Guided Wave Letters*, vol. 9, no. 10, pp. 404–406, Oct 1999.
- [5] J.-S. Zhan and J.-L. Wang, "A simple four-order cross-coupled filter with three transmission zeros," *Progress In Electromagnetics Research*, vol. 8, pp. 57–68, 2009.
- [6] W. Shen, L.-S. Wu, X.-W. Sun, W.-Y. Yin, and J.-F. Mao, "Novel substrate integrated waveguide filters with mixed cross coupling (mcc)," *IEEE Microwave and Wireless Components Letters*, vol. 19, no. 11, pp. 701–703, Nov 2009.
- [7] K. Gong, W. Hong, Y. Zhang, P. Chen, and C. J. You, "Substrate integrated waveguide quasi-elliptic filters with controllable electric and magnetic mixed coupling," *IEEE Transactions on Microwave Theory and Techniques*, vol. 60, no. 10, pp. 3071–3078, Oct 2012.
- [8] E. Naglich, D. Peroulis, and W. Chappell, "Wide spurious free range positive-to-negative inter-resonator coupling structure for reconfigurable filters," in *IEEE MTT-S International Microwave Symposium Digest*, June 2013, pp. 1–4.
- [9] A. Anand and X. Liu, "Capacitively tuned electrical coupling for reconfigurable coaxial cavity bandstop filters," in *IEEE MTT-S International Microwave Symposium Digest*, May 2015, pp. 1–3.
- [10] A. Guyette, "Alternative architectures for narrowband varactor-tuned bandpass filters," in *European Microwave Integrated Circuits Conference*, Sept 2009, pp. 475–478.
- [11] P. Wong and I. Hunter, "Electronically reconfigurable microwave bandpass filter," *IEEE Transactions on Microwave Theory and Techniques*, vol. 57, no. 12, pp. 3070–3079, Dec 2009.
- [12] C. H. Kim and K. Chang, "Ring resonator bandpass filter with switchable bandwidth using stepped-impedance stubs," *IEEE Transactions on Microwave Theory and Techniques*, vol. 58, no. 12, pp. 3936–3944, Dec 2010.
- [13] Y.-C. Chiou and G. Rebeiz, "A tunable three-pole 1.5–2.2-ghz bandpass filter with bandwidth and transmission zero control," *IEEE Transactions on Microwave Theory and Techniques*, vol. 59, no. 11, pp. 2872–2878, Nov 2011.
- [14] H.-J. Tsai, N.-W. Chen, and S.-K. Jeng, "Center frequency and bandwidth controllable microstrip bandpass filter design using loop-shaped dual-mode resonator," *IEEE Transactions on Microwave Theory and Techniques*, vol. 61, no. 10, pp. 3590–3600, Oct 2013.
- [15] J.-R. Mao, W.-W. Choi, K.-W. Tam, W. Q. Che, and Q. Xue, "Tunable bandpass filter design based on external quality factor tuning and multiple mode resonators for wideband applications," *IEEE Transactions on Microwave Theory and Techniques*, vol. 61, no. 7, pp. 2574–2584, July 2013.
- [16] Y. Deng and K. Wu, "Compact bandpass filter with tunable center frequency and reconfigurable bandwidth," in *European Microwave Conference*, Oct 2013, pp. 1027–1030.
- [17] Y.-H. Cho and G. Rebeiz, "Two- and four-pole tunable 0.7–1.1-ghz bandpass-to-bandstop filters with bandwidth control," *IEEE Transactions*

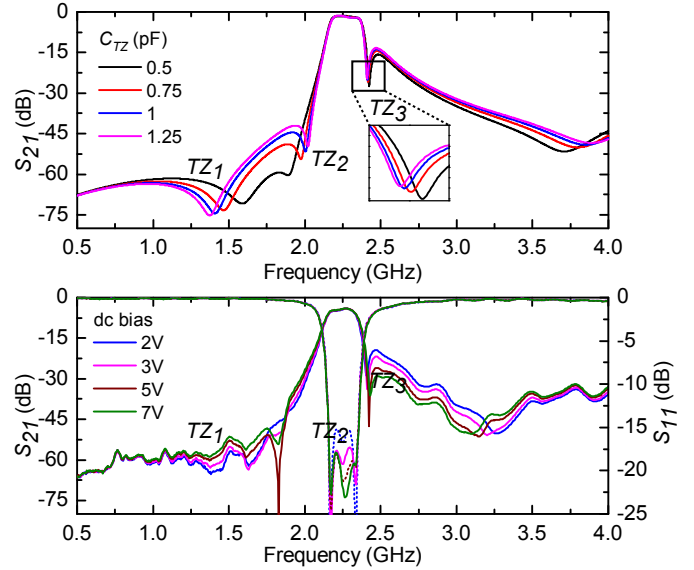
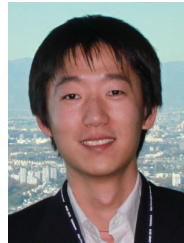


Fig. 26. (a) Simulated and (b) measured s-parameters of four-pole filter showing tunable TZs.

- on Microwave Theory and Techniques*, vol. 62, no. 3, pp. 457–463, March 2014.
- [18] C.-C. Cheng and G. Rebeiz, “High-q 4-6 ghz suspended stripline rf mems tunable filter with bandwidth control,” *IEEE Transactions on Microwave Theory and Techniques*, vol. 59, no. 10, pp. 2469–2476, Oct 2011.
- [19] A. Anand and X. Liu, “Substrate-integrated coaxial-cavity filter with tunable center frequency and reconfigurable bandwidth,” in *Wireless and Microwave Technology Conference (WAMICON), 2014 IEEE 15th Annual*, June 2014, pp. 1–4.
- [20] T. Yang, K. Ho, and G. Rebeiz, “Compact self-shielded 2–3 ghz high-q coaxial fixed and tunable filters,” *IEEE Transactions on Microwave Theory and Techniques*, vol. 62, no. 12, pp. 3370–3379, Dec 2014.
- [21] R. J. Wenzel, “Exact design of wideband equal-ripple bandpass filters with non-adjacent resonator couplings,” in *IEEE-MTT-S International Microwave Symposium*, June 1976, pp. 125–127.
- [22] L. Szydlowski, A. Lamecki, and M. Mrozowski, “Coupled-resonator waveguide filter in quadruplet topology with frequency-dependent coupling-a design based on coupling matrix,” *IEEE Microwave and Wireless Components Letters*, vol. 22, no. 11, pp. 553–555, Nov 2012.
- [23] R. Levy, “Filters with single transmission zeros at real or imaginary frequencies,” *IEEE Transactions on Microwave Theory and Techniques*, vol. 24, no. 4, pp. 172–181, Apr 1976.
- [24] A. D. Lapidus and C. Rossiter, “Cross-coupling in microwave bandpass filters,” *Microwave Journal*, vol. 47, no. 11, pp. 22–46, Nov 2004.
- [25] J. Martinez, M. Taroncher, and V. Boria, “Capacitively loaded resonator for compact substrate integrated waveguide filters,” in *European Microwave Conference*, Sept 2010, pp. 192–195.
- [26] I. Hunter, *Theory and Design of microwave Filters*. London, United Kingdom: The Institution of Electrical Engineers, 2001.
- [27] S. Sirci, J. Martinez, M. Taroncher, and V. Boria, “Varactor-loaded continuously tunable siw resonator for reconfigurable filter design,” in *European Microwave Conference*, Oct 2011, pp. 436–439.
- [28] ——, “Analog tuning of compact varactor-loaded combline filters in substrate integrated waveguide,” in *European Microwave Conference*, Oct 2012, pp. 257–260.
- [29] A. Anand, J. Small, M. S. Arif, M. Sinani, D. Peroulis, and X. Liu, “A novel high-qu octave-tunable resonator with lumped tuning elements,” in *IEEE MTT-S International Microwave Symposium Digest*, June 2013, pp. 1–3.
- [30] A. Anand, Y. Liu, and X. Liu, “Substrate-integrated octave-tunable combline bandstop filter with surface mount varactors,” in *Wireless Symposium (IWS), 2014 IEEE International*, March 2014, pp. 1–4.
- [31] A. Anand, J. Small, D. Peroulis, and X. Liu, “Theory and design of octave tunable filters with lumped tuning elements,” *IEEE Transactions on Microwave Theory and Techniques*, vol. 61, no. 12, pp. 4353–4364, Dec 2013.
- [32] H. Wang and Q.-X. Chu, “Generation of transmission zero through electric and magnetic mixed coupling,” in *International Conference on Microwave and Millimeter Wave Technology*, April 2007, pp. 1–3.
- [33] J.-S. Hong, *Microstrip Filters for RF/Microwave Applications*. New York: Wiley, 2011.
- [34] D. Swanson, “Narrow-band microwave filter design,” *IEEE Microwave Magazine*, vol. 8, no. 5, pp. 105–114, Oct 2007.
- [35] D. Deslandes and K. Wu, “Analysis and design of current probe transition from grounded coplanar to substrate integrated rectangular waveguides,” *IEEE Transactions on Microwave Theory and Techniques*, vol. 53, no. 8, pp. 2487–2494, Aug 2005.
- [36] A. Atia and A. Williams, “Narrow-bandpass waveguide filters,” *IEEE Transactions on Microwave Theory and Techniques*, vol. 20, no. 4, pp. 258–265, Apr 1972.
- [37] J. Thomas, “Cross-coupling in coaxial cavity filters - a tutorial overview,” *IEEE Transactions on Microwave Theory and Techniques*, vol. 51, no. 4, pp. 1368–1376, Apr 2003.
- [38] X. Wang, G. Jang, B. Lee, and N. Park, “Compact quad-mode bandpass filter using modified coaxial cavity resonator with improved q -factor,” *IEEE Transactions on Microwave Theory and Techniques*, vol. 63, no. 3, pp. 965–975, March 2015.
- [39] M. El-Tanani and G. Rebeiz, “A two-pole two-zero tunable filter with improved linearity,” *IEEE Transactions on Microwave Theory and Techniques*, vol. 57, no. 4, pp. 830–839, April 2009.



Aakash Anand (S’12) received the B.S. degree in electrical engineering from University of California, Davis in 2009. He is currently working towards his Ph.D. degree at University of California, Davis. His research interest includes RF/microwave tunable filters, RF and analog IC design, and reconfigurable RF systems.



Dr. Xiaoguang “Leo” Liu (S’07–M’10) received his B.S. degree from Zhejiang University, China in 2004 and his Ph.D. degree from Purdue University in 2010. He is currently an assistant professor in the Department of Electrical and Computer Engineering at the University of California, Davis. His research interests include RF-MEMS and other reconfigurable RF/microwave components, software defined radios, and terahertz components and systems. He has published over 30 papers in peer-reviewed journals and conferences. As a student, he received the graduate research fellowship from IEEE Antenna and Propagation Society in 2009. He was selected as a UC Davis Hellman Fellow in the 2013–2014 academic year.